Affinity-controlled capture and release of engineered monoclonal antibodies by macroporous dextran hydrogels using coiled-coil interactions

Seyed Farzad Baniahmad, Romane Oliverio, Ines Obregon-Gomez, Alma Robert, Anne E.G. Lenferink, Elena Pazos, Nick Virgilio, Xavier Banquy, Gregory De Crescenzo & Yves Durocher

View supplementary material

Published online: 10 Jun 2023.

Submit your article to this journal

Article views: 900

View related articles

View Crossmark data

Taylor & Francis
Taylor & Francis Group

REPORT

🔓 OPEN ACCESS | Check for updates

Affinity-controlled capture and release of engineered monoclonal antibodies by macroporous dextran hydrogels using coiled-coil interactions

Seyed Farzad Baniahmad[a,b], Romane Oliverio[c,d], Ines Obregon-Gomez[e], Alma Robert[b], Anne E.G. Lenferink[b], Elena Pazos[e], Nick Virgilio[f], Xavier Banquy[d], Gregory De Crescenzo[c*], and Yves Durocher [ORCID][a,b*]

aDepartment of Biochemistry and Molecular Medicine, Faculty of Medicine, University of Montreal, Montreal, QC, Canada; bHuman Health Therapeutics Research Centre, Building Montreal-Royalmount, National Research Council Canada, Montréal, Québec, Canada; cDepartment of Chemical Engineering Polytechnique Montréal, Montréal, Québec Canada; dFaculty of Pharmacy, Axe Formulation Et Analyse du Médicament, Université de Montréal, Québec, Canada; eCICA - Centro Interdisciplinar de Química E Bioloxía and Departamento de Química, Facultade de Ciencias, Universidade da Coruna, Coruna, Spain; fDepartment of Chemical Engineering, Centre de Recherche Sur Les Systèmes Polymères Et Composites à Haute Performance (CREPEC), Montréal, Canada

ABSTRACT

Long-term delivery is a successful strategy used to reduce the adverse effects of monoclonal antibody (mAb)-based treatments. Macroporous hydrogels and affinity-based strategies have shown promising results in sustained and localized delivery of the mAbs. Among the potential tools for affinity-based delivery systems, the de novo designed Ecoil and Kcoil peptides are engineered to form a high-affinity, heterodimeric coiled-coil complex under physiological conditions. In this study, we created a set of trastuzumab molecules tagged with various Ecoil peptides and evaluated their manufacturability and characteristics. Our data show that addition of an Ecoil tag at the C-termini of the antibody chains (light chains, heavy chains, or both) does not hinder the production of chimeric trastuzumab in CHO cells or affect antibody binding to its antigen. We also evaluated the influence of the number, length, and position of the Ecoil tags on the capture and release of Ecoil-tagged trastuzumab from macroporous dextran hydrogels functionalized with Kcoil peptide (the Ecoil peptide-binding partner). Notably, our data show that antibodies are released from the macroporous hydrogels in a biphasic manner; the first phase corresponding to the rapid release of residual, unbound trastuzumab from the macropores, followed by the affinity-controlled, slow-rate release of antibodies from the Kcoil-functionalized macropore surface.

Introduction

Monoclonal antibodies (mAbs) are one of the most successful tools available for cancer therapy. Currently, more than 100 antibodies have been approved by the US Food and Drug Administration. Since the approval of muromonab-CD3 (Orthoclone; Ortho Biotech) in 1986 as the first therapeutic mAb for use in humans, these proteins have been applied to the treatment of oncological, immunological, and infectious diseases.[1–3] Parenteral injections are the preferred route of administration for most antibodies. Among all, the intravenous injection is superior in terms of pharmacokinetic and pharmacodynamic efficacy of drug delivery to the body, and is comparatively less immunogenic.[4] However, to obtain restorative benefits and therapeutic advantages and compensate for the dose-dependent elimination, antibodies must be delivered either in large doses or by multiple injections at short intervals. For instance, trastuzumab (TZM) which is used in the adjunctive treatment of human epidermal growth factor receptor (HER2)-overexpressing breast cancer can be administered in some cases up to 3 times a week over a year.[5] In addition to the high cost of such treatment, this may result in side effects and negative health outcomes, and compromise patient compliance.[5–7]

To reduce the frequency of administrations, increase the effect at the site of interest, and improve pharmacokinetic efficacy, novel drug delivery systems enabling sustained and localized mAb release have been developed. Nanoparticle-mediated delivery of anti-OX40 mAb,[8] enhancement of osteogenesis by using anti-BMP2 mAb encapsulated in alginate microspheres,[9] and use of thermo-sensitive hydrogel as an intraocular delivery system for bevacizumab intravitreal injection, are some of the successful developments.[10]

Encapsulating therapeutics, including mAbs, in hydrogels for localized and controlled drug delivery has been tried for more than a decade.[11,12] In most cases, the release relies on the pattern of gel degradation and the control over the release is limited. Macroporous hydrogels and scaffolds, where a secondary macropore (>10 µm) network crosses the main hydrogel mesh, have also emerged as an alternative.[13,14] Macroporous scaffolds are designed to offer a large pore surface area, and for the expected interactions to occur in macropores rather than in the hydrogel mesh. These features make macroporous scaffolds suitable for post-crosslinking loading and reloading with a wide

range of bioactive components of various sizes.[15,16] Macroporous hydrogels can be covalently crosslinked in potentially harsh chemical conditions, to provide easy-to-handle, robust materials. However, to be used in controlled release applications, they must be functionalized to prevent immediate release of the component into the environment.

To address this obstacle, one possible avenue is the use of affinity-based strategies, to limit the burst release and improve control. The use of an affinity-based platform provides more control over the release of the drug than passive hydrogel erosion.[17,18] Numerous studies have focused on the development of both bulk and macroporous hydrogels for the controlled delivery of various biological therapeutics, such as growth factors[15,19,20] or mAbs,[21,22] using affinity-based strategies such as aptamers,[20] affinity peptides,[15,19] or biotin–avidin interactions.[21,22] Notably, Huynh and Wylie proposed both streptavidin-antibody conjugates for competitive release from desthiobiotinylated hydrogels[21] and desthiobiotinylated antibodies for displacement affinity release from neutravidin-conjugated hydrogels.[22]

Affinity peptides are versatile tunable tools that can be easily expressed as tags on recombinant proteins. This strategy ensures the efficient tagging of the protein since no extra conjugation step is required and removes the need for an additional purification step. Coiled-coil peptides are commonly used affinity systems derived from the coiled-coil structure, which is one of the most abundant naturally occurring motifs for protein folding and assembly.[17] Structurally, this oligomerization motif consists of two or more α helices wrapped around each other. It is commonly found in many proteins involved in cellular activities, including transcription, muscle contractions, or viral fusion mechanisms.[23–25] The fingerprint of this structure is a repeat of a seven-residue motif (heptad), the number of which can vary from 200 in naturally occurring fibrous proteins to only two heptads in a *de novo* designed synthetic coiled-coil.[26] The E/K coiled coil is a *de-novo*-designed coiled-coil in which the Ecoil and Kcoil peptides, heptads: EVSALKE (Ecoil) and KVSALEK (Kcoil), form a highly specific, heterodimeric coiled-coil interaction with a high affinity, shown to be sufficiently strong in physiological conditions.[27,28]

We recently reported the design of an affinity-controlled capture and delivery system from a macroporous dextran hydrogel for two growth factors.[15] In this work, the Kcoil peptide was conjugated to the surface of macroporous templated dextran hydrogels, with a macropore size in the 100 μm range and high (>95%) macropore interconnectivity. These Kcoil-functionalized hydrogels were used for the loading and subsequent release of Ecoil-tagged epidermal- and vascular endothelial growth factors (EGF, VEGF). We have shown that this highly tunable platform is able to deliver a bioactive Ecoil-tagged EGF up to 96 hours post-loading in a cell proliferative assay.[15] Results from this work provide promising perspectives on controlled drug delivery systems. The use of a macroporous platform, where protein diffusion is controlled by the E/K affinity pair and mainly occurs in the macropore network of the gel rather than in the hydrogel mesh, suggests a versatile delivery system for different therapeutic proteins, regardless of their size.

Here, we focus on the design, production, and purification of a set of Ecoil-tagged trastuzumab (TZM) analogs by transient transfection of a Chinese hamster ovary (CHO) cell line. More specifically, we produced nine different constructs corresponding to TZM bearing a *C*-terminal Ecoil-tag on its light chains (HC-LCx), its heavy chains (HCx-LC) or both (HCx-LCx), where x, being equal to 3, 4, or 5, corresponds to the number of heptads in the Ecoil sequence. We verified the manufacturability and characterized all nine modified TZMs using both analytical and cell-based assays. We analyzed the influence of the number, length, and position of the Ecoil tags on the bioactivity of the antibodies. Finally, we studied the capture and controlled release of the Ecoil-tagged TZMs using the Kcoil-functionalized macroporous dextran hydrogels we previously developed.[15]

Results

Production, purification, and characterization of the Ecoil-tagged TZMs

In this work, we produced Ecoil-tagged recombinant mAbs. The chosen antibody, trastuzumab (TZM), was modified to express a *C*-terminal Ecoil tag on heavy chains (HCx-LC), light chains (HC-LCx) or both (HCx-LCx) (Figure 1), where x stands for the number of (EVSALEK) heptads — 3, 4 or 5 — in the Ecoil sequence.

All antibodies were produced at a 250 mL scale in a transient CHO-3E7 expression system, using 1 L Erlenmeyer ventilated shake flasks.[29] Wild type (pristine) trastuzumab was produced similarly and used as control. Primary characterization by sodium dodecyl sulfate – polyacrylamide gel electrophoresis (SDS-PAGE) analysis on the harvested supernatants 10 days post-transfection shows a band below the corresponding molecular weight of 250 kDa (shown in Figure 2A, lane 2 for HC5-LC5), thus confirming the production of the chimeric antibodies.

Prior to the purification, we measured the final titer of the Ecoil-tagged TZMs in the filtered supernatant by protein-A high-performance liquid chromatography (HPLC) and thus investigated the effect of the Ecoil tags on the production yield. All Ecoil-tagged antibodies were obtained at yields of 163–283 mg/L, compared to the production yield of 217 mg/L for TZM (Table 1). The lowest titer (163 mg/L) corresponded to antibody expressing E coil tag with 4 heptads at both light and heavy chains (HC4-LC4). The second lowest titer was for HC5-LC5 (170 mg/L), and the titers of the other chimeric TZM were found to be similar to that of the TZM control. These results indicate that the presence of *C*-terminal Ecoil tags does not significantly affect the chimeric TZM production.

The harvested supernatants were then purified by protein-A affinity chromatography. The SDS-PAGE migration profiles of the eluted fractions are shown for HC5-LC5 in Figure 2A, lanes 3–7. The fractions were then pooled, and the buffer was exchanged for phosphate-buffered saline (PBS), leading to the final product (Figure 2A, lane 8). Compared to lane 2, lanes 3–8 show an increased relative intensity of the main band (positioned below 250 kDa), corresponding to the HC5-LC5
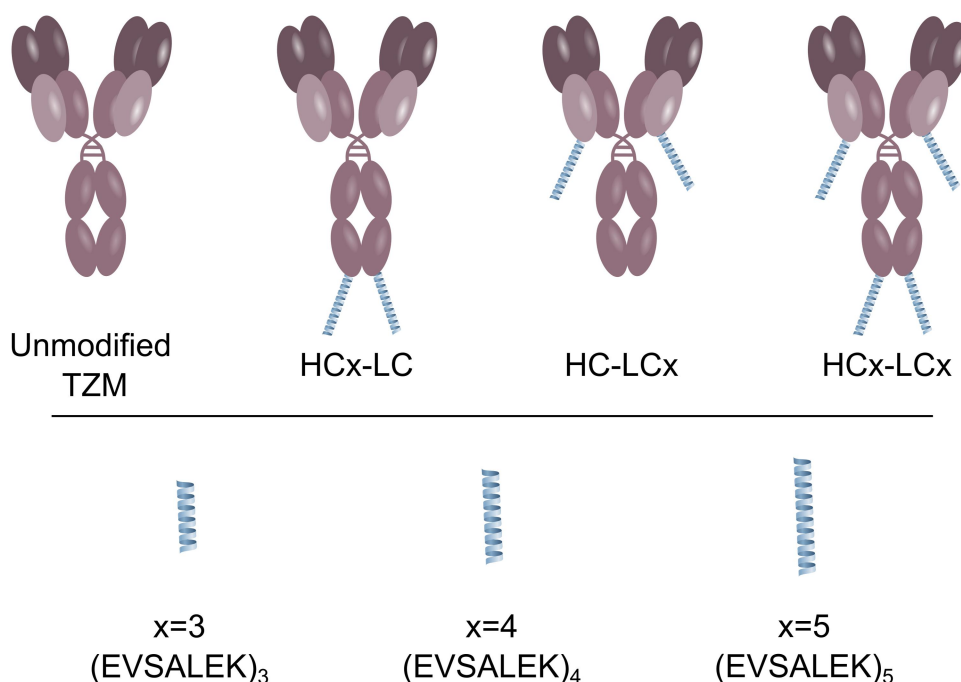
Figure 1. Nomenclature of the various tagged TZM antibodies. The Ecoil tags are located at the C-terminus of the heavy chains (HCx-LC), light chains (HC-LCx), or both (HCx-LCx). The Ecoil tags contain x = 3, 4 or 5 heptads.

antibody. However, several unexpected extra bands were still observed in lanes 3–8, as well as on lane 9 (pristine TZM). All these lanes exhibit a similar migration pattern (with a down shift related to the absence of the Ecoil tag), with the extra bands ranging from ~ 25–150 kDa. Since no such species are detected during the size-exclusion chromatography (SEC)-ultra-performance liquid chromatography (UPLC) analyses, these bands are more likely artifacts coming from the SDS-PAGE sample preparation process and protein migration under non-reducing conditions, as reported in previous studies.[30–32] Indeed, these studies suggested that free sulfhydryl groups in the antibodies could catalyze disulfide bond scrambling and result in antibody fragmentation. The addition of reducing agents in the SDS-PAGE sample buffer is expected to prevent such fragment-band artifacts. Indeed, in reducing conditions (Figure 2A, lanes 10 and 11), we observe the disappearance of most unexpected bands. Altogether (Figure 2A, Figure S1 and data not shown), these observations indicated the efficient concentration and purification of our chimeric antibodies.

While the differences in observed molecular weight between the light and heavy chains of HC5-LC5 and unmodified TZM strongly suggested the successful addition and expression of the Ecoil tags, these observations were further confirmed by multi-angle light scattering (MALS) analysis and SDS-PAGE (Figure 2B), which provided an estimate of the molecular weight and proof of the increase in the light and heavy chains' molecular weights as a result of the tag addition. MALS data were found to be consistent with the theoretical molecular weight (ProtParam tool – Expasy, Table 1), with an observed molecular weight increment for all Ecoil-tagged antibodies compared to wild-type trastuzumab. Additionally, the SDS-PAGE migration profiles of the three different Ecoil-

tagged antibodies in Figure 2B evidence the differences between 3-, 4- and 5-heptad-long Ecoil tags and their impact on the molecular weight of both heavy and light chains. In addition, UPLC-SEC analysis (Table 1) indicated that the purities of the final products were similar to that of the control and above 97%, except for the HC5/LC5 chimera, which contained approximately 10% aggregates.

Bioactivity of the Ecoil-tagged TZMs

We then investigated the ability of the Ecoil-tagged TZMs to bind to their biological target, the membrane-bound receptor tyrosine kinase HER2. More precisely, we evaluated the cell-binding characteristics of the Ecoil-tagged TZMs in a plate-based cell-binding assay.

HER2-positive SK-BR-3 breast cancer cells were incubated with Ecoil-tagged antibodies at concentrations ranging from 0.14 to 300 nM. Pristine TZM and palivizumab (PVZM, Synagis) were used as positive and negative controls, respectively. Triple-negative MDA-MB-231 breast cancer cells were also used as a negative control, to assess the levels of nonspecific binding of the antibodies to the cell surface (Figure S2). Figure 3B shows the immunofluorescent imaging of SK-BR-3 cells in the presence of nuclear (blue) and cell membrane (red) staining dyes. The green signal corresponds to TZM on the cell surface, detected by the secondary antibody (anti-human AF488-IgG). Untreated SK-BR-3 cells (Figure 3A) were used for background control.

The dose-dependent binding curves (Figure 3C-E) indicated that the Ecoil tags did not hinder the binding capacity of the antibodies to the cell surface receptor. The data were then fitted using the model defined in equation (1), where Y corresponds to the intensity per cell area of the specific
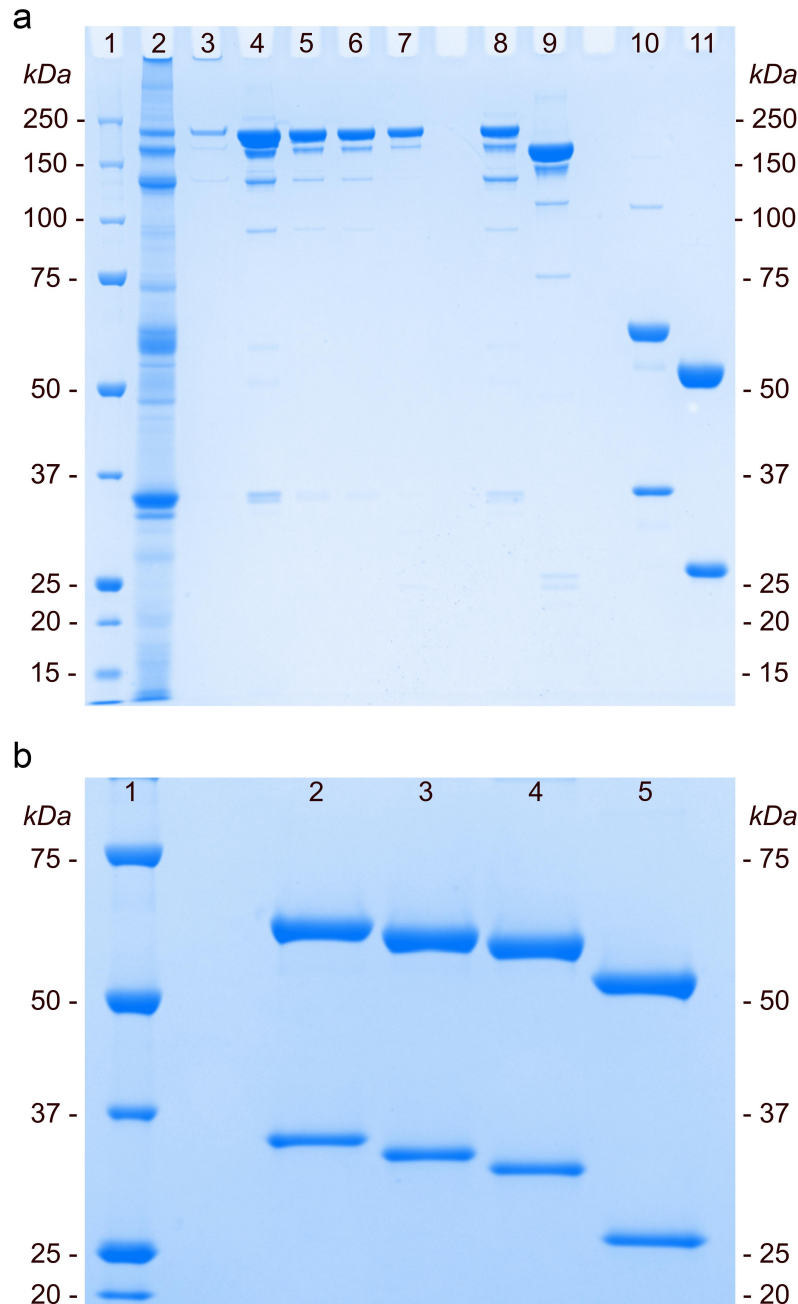
Figure 2. (A) SDS-PAGE characterization of HC5-LC5 (lanes 2–8, 10), compared to wild type TZM (lanes 9, 11). Samples were prepared in both non-reducing (lanes 2–9) and reducing (lanes 10–11) conditions. Lane 1: molecular weight ladder. Lane 2: cell culture supernatant. Lanes 3–7: eluted fractions of the protein-A affinity chromatography column. Lane 8: final product (HC5-LC5). Lane 9: wild-type TZM. Lane 10: reduced HC5-LC5. Lane 11: reduced TZM. (B) SDS-PAGE characterization of HC5-LC5, HC4-LC4 and HC3-LC3 (lanes 2, 3 and 4, respectively), compared to wild type TZM (lane 5) in reducing conditions. Lane 1: molecular weight ladder.

binding, C the antibody concentration, B_{max} the maximum specific binding, h the Hill slope and K_D the dissociation constant.

$$Y = \frac{B_{max} \cdot C^h}{K_D{}^h + C^h} \qquad (1)$$

The calculated values for K_D as the mean of three independent assays are presented in Table 2. B_{max} and h were determined independently for each experiment, and the values

corresponding to the representative dose-binding curves in Figure 3C-E are presented in Table S1.

Very low binding of PVZM to the SK-BR-3 cell membranes (Figure 3C-E), compared to wild-type TZM, and lack of detectable binding signal for tagged-TZMs to the MDA-MB-231 cell surface (Figure S2) confirmed the specificity of the assay.

Although the presence of the Ecoil tags seemed to slightly increase the K_D of the TZM/HER2 interaction (Table 2), especially when four Ecoil-tags are present (HCx-LCx), this trend was not confirmed by statistical analysis (i.e., $p > 0.05$

Table 1. Titer in supernatants and SEC-MALS characterization of Ecoil-tagged TZMs.

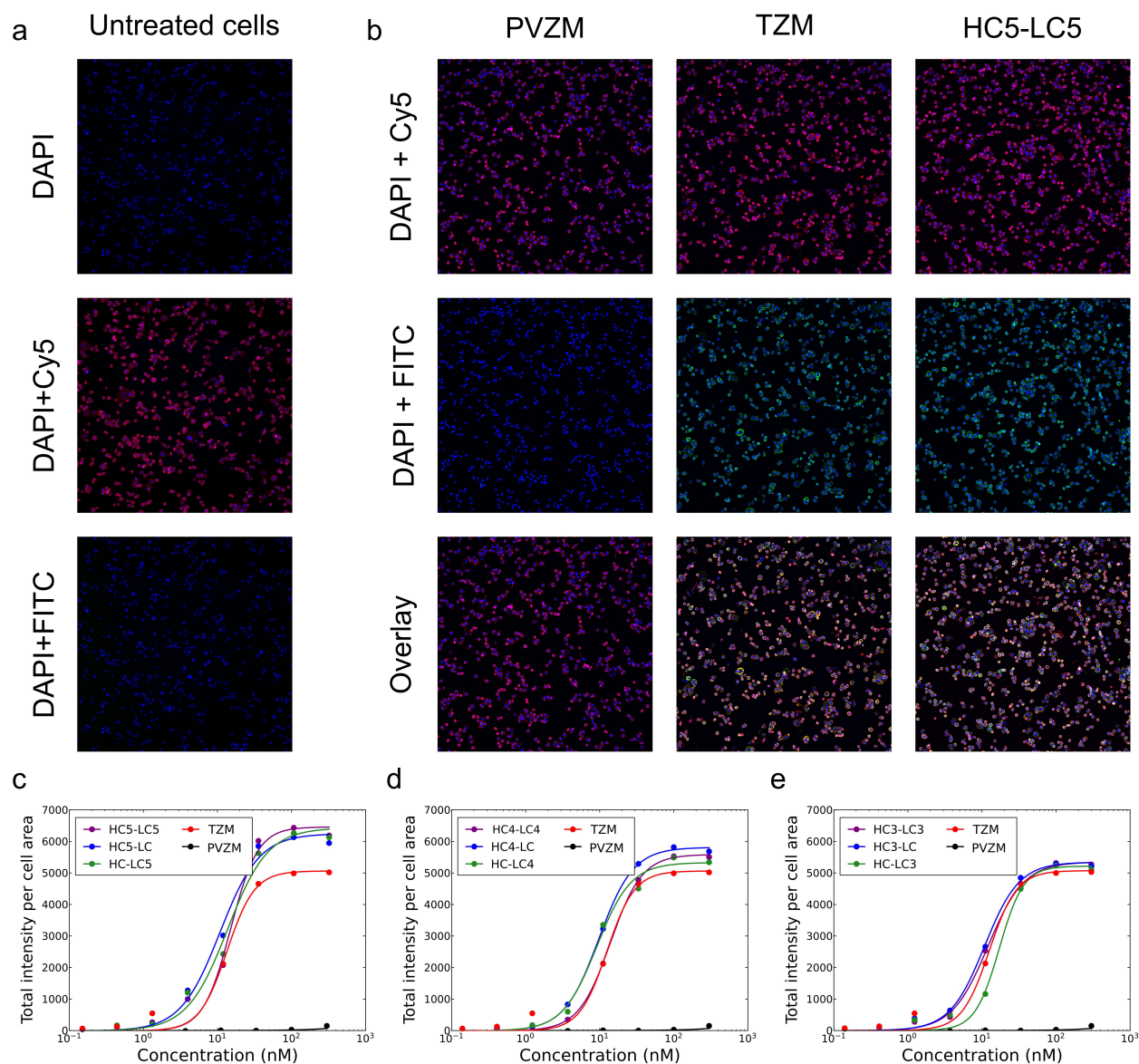|	Titer in supernatant (mg/L)	Purity (% of monomers)	Theoretical molecular weight (M_W, kDa)	Molecular weight (M_{MALS}, kDa)
HC5-LC5	170	91.5	165	155.7
HC5-LC	202	98.3	155	145.6
HC-LC5	192	98.4	155	152.8
HC4-LC4	163	97.9	162	157.1
HC4-LC	178	97.7	153	148.6
HC-LC4	178	98.6	153	144.3
HC3-LC3	264	97.7	159	154.6
HC3-LC	283	98.3	152	148.1
HC-LC3	219	98.3	152	146.3
TZM	217	98.8	145	137.3

Figure 3. Cellular analysis of the binding of Ecoil-tagged TZM to its biological partner HER2. (A) Untreated SK-BR-3 cells were used as a background control (blue: cell nuclei, red: cell membranes, green: antibodies). (B) Representative, processed images showing the binding of TZM and HC5-LC5 (green) to HER2, compared to the negative control PVZM. Images are taken with a 4X objective. (C-E) Dose-dependent binding curves of E5-tagged TZM (C), E4-tagged TZM (D) and E3-tagged TZM (E). All Ecoil-tagged TZM exhibited similar cell binding behaviors as unmodified TZM. Negative control PVZM does not bind SK-BR-3 cells.

for all pairwise comparisons to unmodified TZM). Overall, the binding remained very effective, since the K_D values were all in the low nanomolar range and similar to that of the pristine TZM.

Altogether, we demonstrated that Ecoil-tagged TZMs retained their ability to efficiently and specifically bind to HER2 at the cell surface.

Table 2. K_D values (n = 3), obtained by fitting the dose-response curves with Equation 1.

	K_D (nM)
HC5-LC5	12.96 ± 2.08
HC5-LC	7.88 ± 2.15
HC-LC5	8.86 ± 2.78
HC4-LC4	11.89 ± 1.64
HC4-LC	7.99 ± 1.98
HC-LC4	8.69 ± 2.56
HC3-LC3	10.63 ± 2.52
HC3-LC	9.04 ± 3.04
HC-LC3	8.87 ± 3.93
TZM	8.41 ± 3.81

Influence of the number and position of the Ecoil tags on the interaction with the K5 peptide

To assess how the number (2 or 4) and the position (light chains, heavy chains, or all of them) of the various Ecoil tags influence how the chimeric TZMs interact with Kcoil, we designed a surface plasmon resonance (SPR) assay in which E5- and E4-tagged antibodies were injected on a K5-functionalized sensor chip. The purpose of this assay was to assess the dissociation kinetics of the antibodies when they are bound to a Kcoil-functionalized surface. We attempted to perform the same evaluation for the E3-tagged antibodies but were not able to capture enough E3-TZM to perform the analysis (Figure S3).

Of interest is that the sensor chip was functionalized with 15 resonance units (RU) of K5 peptide, which represented an average distance of ~20 nm between two K5 moieties, assuming that 1 RU corresponded to ~ 1 pg/mm^2, as for globular proteins.[33] This low surface coverage ensured that two Ecoil tags within the same antibody could not simultaneously bind to two different K5 peptides. However, it did not *a priori* prevent the two Ecoils from the same antibody to simultaneously interact with the same K5 peptide.

The recorded sensorgrams are presented in Figure 4 A-C (E5-TZMs) and Figure 5 A-C (E4-TZMs). First, various concentrations of the Ecoil-tagged antibodies were injected on the surface (t < 240s) to interact with K5. The binding of the antibodies to the surface induced an increase in RU, correlated to the amount bound. Then, antibody injection was stopped and replaced by buffer injection (HBS-EP, t > 240s) and dissociation of the E5-TZM/K5 complexes was monitored. During dissociation, the sensorgrams exhibited two phases: an initial, rapid decrease (240s < t < 500s), followed by a slower, steady dissociation (t > 500s). Interestingly, the initial rapid decrease was more strongly marked for HC-LCx (Figures 4C and 5C), and, to a lesser extent, HCx-LCx antibodies (Figures 4A and 5A). We hypothesize this phenomenon to be caused by a lower probability for antibodies bound via their light chain to immediately rebind to the same K5 after initial dissociation. Indeed, as represented in Figure 1, Ecoil tags on heavy chains are closer to one another than on light chains. The existence of these two distinct phases prevented fitting the data with a simple model over the whole dissociation phase. However, the rapid decrease occurred during the first minutes of the dissociation phase and is therefore of lesser interest in long-term release applications. For this reason, we focused the analysis on the second part of the dissociation phase (t > 500s).

Under the hypothesis of a 1:1 interaction, where one antibody is bound to one K5 moiety at a time, the dissociation phase could be modeled as an exponential decay, as represented by equation (2), where $k_{off,app}$ is the apparent kinetic dissociation rate constant.

$$R(t) = R(t_0) \cdot e^{-k_{off,app} \cdot (t-t_0)} \qquad (2)$$

Such was the case experimentally, as shown in Figures 4D-F and 5D-F, where we normalized all SPR responses to $t_0 = 500s$ and applied a logarithmic transformation. The corresponding calculated $k_{off,app}$ are given in Table 3.

$$-\ln\left(\frac{R(t)}{R(t_0)}\right) = k_{off,app} \cdot (t - t_0) \qquad (3)$$

For both E4 and E5 tags, TZMs with four Ecoil tags exhibited smaller values for $k_{off,app}$ than their counterparts harboring only two tags, roughly by a factor 2 (Table 3). When only two Ecoil tags are present, their position (light chain or heavy chain only) had a small impact on the long-term dissociation, with a slightly higher $k_{off,app}$ (<8%) when the tags are located on the light chain.

Modulating the number of heptads of the Ecoil also affected the apparent kinetic dissociation rate constants. That is, replacing E5 by E4 led to an increase in $k_{off,app}$ by a factor 4. When an E3 tag was used, the affinity was too weak for the antibodies to efficiently bind the K5coil-functionalized surface (Figure S2).

Altogether, these results indicate 1) that antibodies harboring four Ecoil tags dissociate more slowly from a K5-functionalized surface than their counterparts harboring only two tags, and 2) that increasing the number of heptads also slows the dissociation.

Bioavailability of immobilized Ecoil-tagged TZMs

To ensure that Ecoil-tagged TZMs engaged in E/K heterodimerization maintained their ability to bind to their antigen HER2, we designed an additional SPR assay, in which HC5-LC5, HC5-LC or HC-LC5 were captured on a K5-functionalized SPR chip, followed by the injection of a chimeric HER2 artificially dimerized by an Fc domain, at various concentrations. The recorded sensorgrams (Figure 6) showed that all three antibodies remained able to bind to HER2. These interactions exhibited high affinity, as shown by the low curvature of the sensorgrams during the injection phase (t < 100s) and the absence of any significant dissociation during the 600 s of HB-EP injection. Of interest, the same amount (95 RU) of HC5-LC and HC-LC5 leads to the capture of slightly less HER2 for HC-LC5 (Figure 6C) compared to HC5-LC (Figure 6B; see Discussion section for further comments). Figure 6A corresponded to 75 RU of HC5-LC5 and thus cannot be quantitatively compared with Figure 6B and c Altogether, all three tagged antibodies remained able to interact with HER2 with high affinity and in a stable fashion, with little to no dissociation observed within 10 minutes of buffer injection.
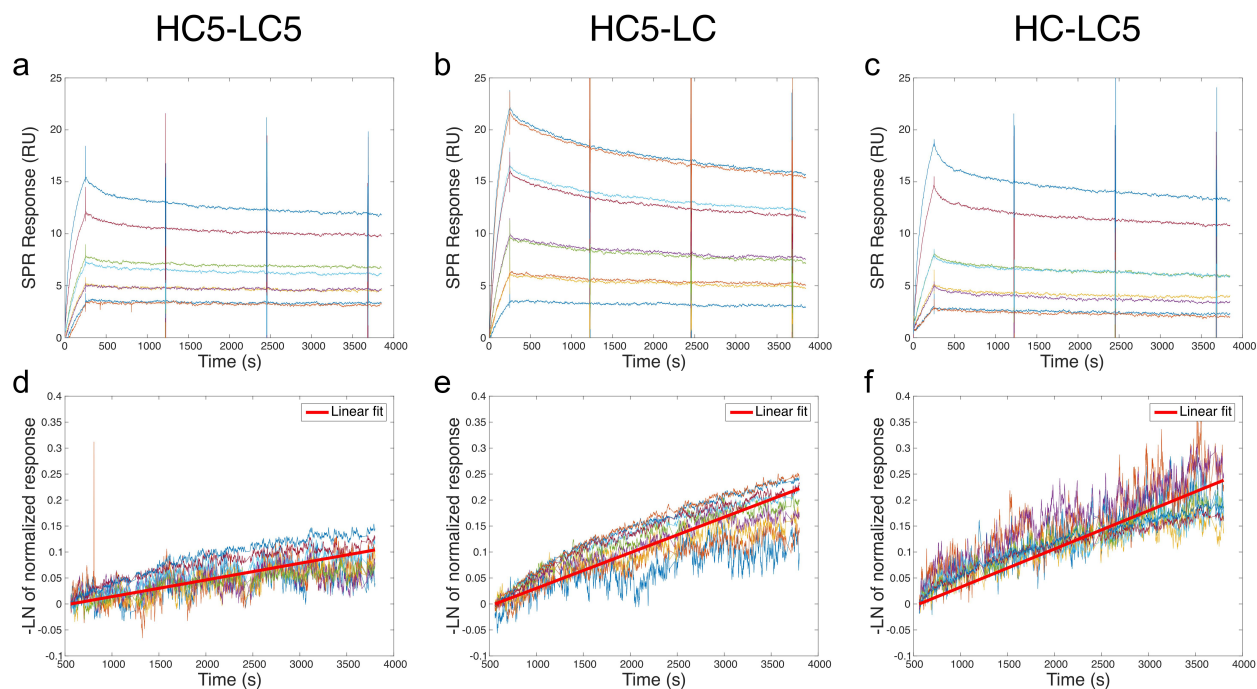
Figure 4. Interaction between the E5-tagged TZMs and K5. (A-C) SPR double-referenced sensorgrams showing the interaction of injected HC5-LC5 (A), HC5-LC (B) and HC-LC5 (C) with the K5-functionalized SPR sensor surface. E5-tagged TZMs are injected at concentrations of 2.5, 5, 10, 25 and 50 nM. (D-F) Logarithm of the normalized SPR responses during the second part of the dissociation phase ($t > 500s$) for HC5-LC5 (D), HC5-LC (E) and HC-LC5 (F). The slope of the linear fit has a value of $k_{off,app}$, according to equation (3).

Figure 5. Interaction between the E4-tagged TZMs and K5. (A-C) SPR double-referenced sensorgrams showing the interaction of injected HC4-LC4 (A), HC4-LC (B) and HC-LC4 (C) with the K5-functionalized SPR chip. E4-tagged TZMs are injected at concentrations of 25, 50, 100, 250 and 500 nM. (D-F) Logarithm of the normalized SPR responses during the second part of the dissociation phase ($t > 500s$) for HC4-LC4 (D), HC4-LC (E) and HC-LC4 (F). The slope of the linear fit has a value of $k_{off,app}$, according to equation (3).
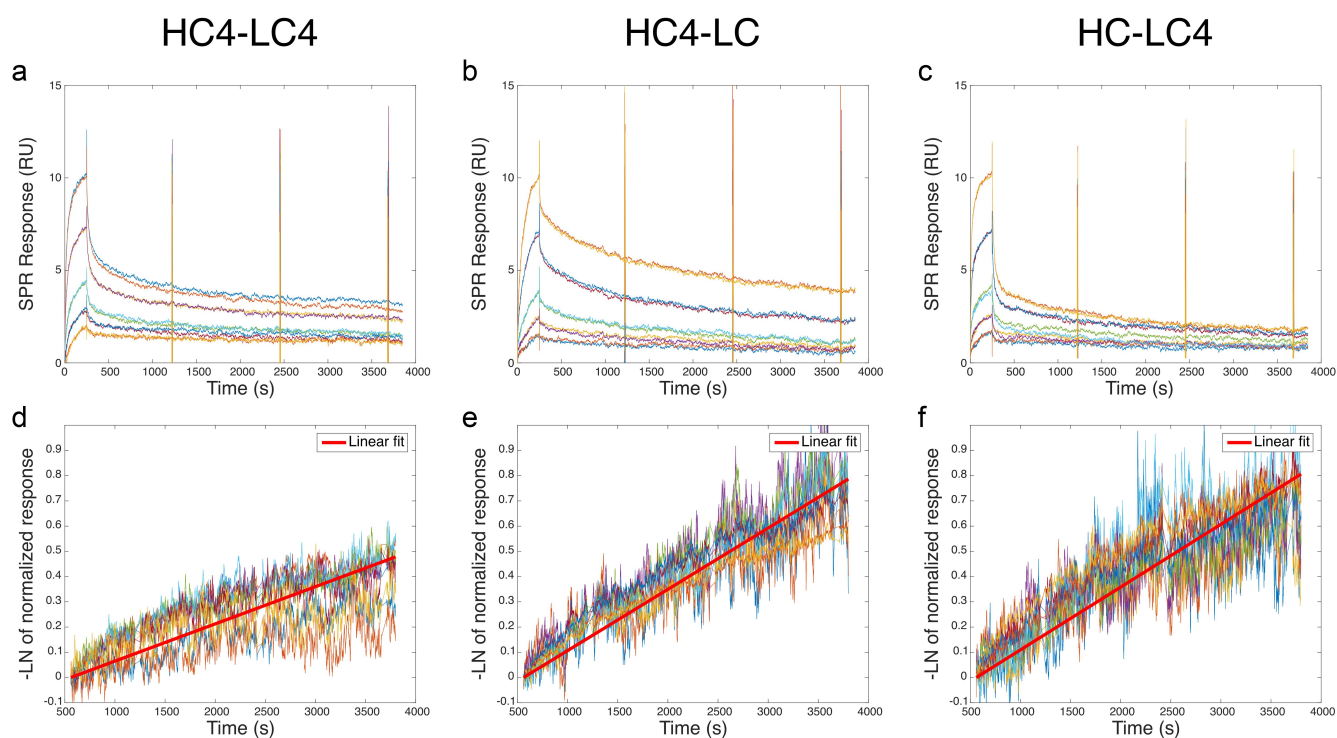
Table 3. Apparent kinetic dissociation rate constants $k_{off,app}$ for the interaction between K5 and Ecoil-tagged TZMs, as determined from the SPR sensorgrams shown in Figures 4 and 5.

	$k_{off,app}$ (s^{-1})		$k_{off,app}$ (s^{-1})
HC5-LC5	3.21×10^{-5}	HC4-LC4	1.48×10^{-4}
HC5-LC	6.85×10^{-5}	HC4-LC	2.43×10^{-4}
HC-LC5	7.35×10^{-5}	HC-LC4	2.49×10^{-4}

Influence of the number and position of the tags on the capture and release of TZM by macroporous dextran hydrogels

We then analyzed the capture and subsequent release of Ecoil-tagged TZM by macroporous dextran hydrogels, for the setup of an affinity-based controlled release platform for the delivery of antibodies. For this purpose, we relied on the approach we previously published,[15] in which the amount of covalently immobilized Kcoil peptide could be modulated.

Briefly, macroporous dextran hydrogels were generated by crosslinking a dextran solution, molded into a polylactic acid (PLA) macroporous scaffold, using trisodium trimetaphosphate (STMP) as a crosslinking agent (Figure 7A). After the selective dissolution of the PLA scaffold in chloroform and subsequent swelling of the gels in PBS, the gels were functionalized with 0.5 (10×), 5 (100×) or 50 (1000×) nmol of Aha-K5 (Figure 7B). Confocal microscopy images of macroporous dextran gels functionalized with a fluorescent Aha-K5 confirmed the homogeneous functionalization of the gel (Figure S4A-B).

Once functionalized with the desired amount of Kcoil, the macroporous dextran hydrogels were immersed in 1 mL of a solution containing 50 nM of Ecoil-tagged TZM. Here, the notation "10×", "100×" or "1000×" refers to the molar excess of Kcoil over the antibody. During this incubation period, the Ecoil-tagged TZM distributed between the macropores of the gel and the surrounding medium, to reach an equilibrium characterized by the partition coefficient defined in equation (5). Confocal microscopy images of 100× gels incubated with a fluorescent E5 confirmed the localization of the E/K heterodimers at the surface of the macropores (Figure S4C-E).

After 72 h, the surrounding medium was collected and replaced by fresh PBS-T, thus triggering the dissociation and release of the Ecoil-tagged TZM. PBS-T replacement was repeated after 1 h, 3 h, 24 h, 48 h, 72 h and 96 h.

This experimental setup allowed us to compare the capture and release behaviors of three chimeric TZM: HC5-LC5, HC5-LC and HC-LC5. More specifically, we studied how the combined influence of the number and position of the E5 tags on TZM and the amount of K5 in the gels affected loading and release. To do so, we measured the partition coefficients and cumulative release profiles (Figure 8). Cumulative release is expressed as a percentage of the amount initially loaded with the gels, and the obtained release profiles were normalized to the highest values of each dataset to allow comparison between independent experiments.

The cumulative release profiles of E5-tagged TZMs, presented in Figure 8B, exhibit two phases: 1) a fast release (0 h – 24 h), corresponding to the release of antibodies that are physically present in the macropores without being captured via coiled-coil interactions, followed by 2) a slower, late-phase release (24 h – 96 h). At each time point, the amount of antibodies newly released by the gels $n_{released,[t,t+1]}$ is given by equation (4), where $C_{solution,t}$ and $C_{solution,t+1}$ are the concentration of the solution surrounding the gels, and $V_{solution}$ and V_{pores} the volumes of the surrounding solution and the macropore network, respectively. The amounts of antibodies released during the late phase (24 h – 96 h) are presented in Figure 8C.

$$n_{released,[t,t+1]} = C_{solution,t+1} \cdot \left(V_{solution} + V_{pores} \right) - C_{solution,t} \cdot V_{pores} \quad (4)$$

The first observation was that increasing the amount of K5 in gels led to an increase in the partition coefficients (Figure 8A) and a decrease in the initial release (Figure 8B, 0 h – 24 h).
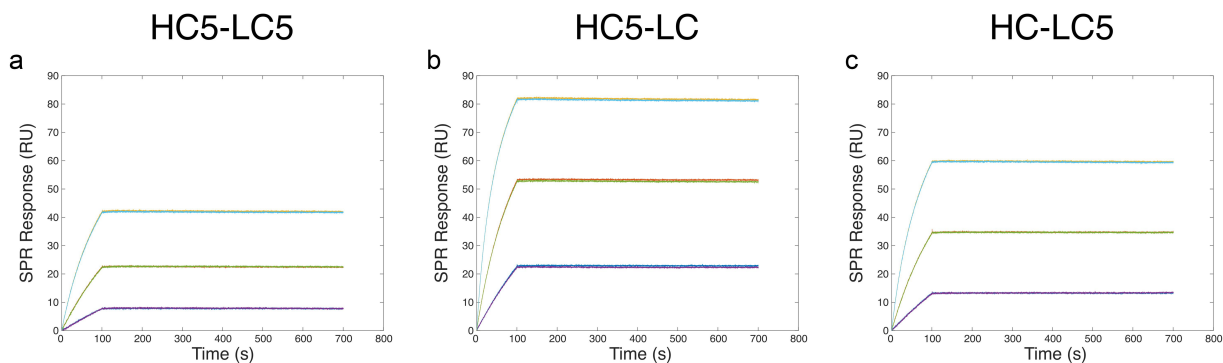

Figure 6. Interaction of soluble HER2 with captured E5-tagged TZMs. (A-C) SPR double-referenced sensorgrams corresponding to the interaction of injected dimeric HER2 with 75 RU of HC5-LC5 (A), 95 RU of HC5-LC (B) and 95 RU of HC-LC5 (C) captured on the SPR chip by coiled-coil interactions. HER2 was injected at concentrations of 3, 10 and 25 nM.
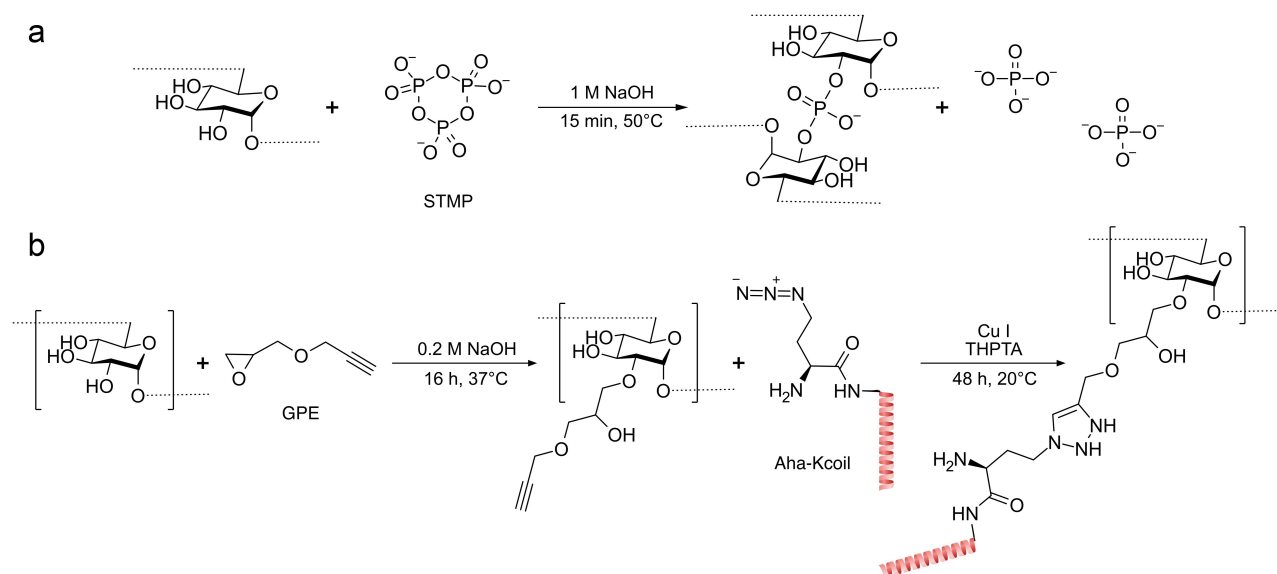
Figure 7. Schemes of the chemical reactions. (A) Crosslinking reaction of dextran. STMP is used as the crosslinking agent and the reaction takes place in alkaline conditions. (B) Chemical grafting of azidohomoalanine-terminated Kcoil to the dextran backbone. Dextran is first incubated with GPE in alkaline conditions to functionalize the dextran with alkyne moieties. Aha-Kcoil is then conjugated by copper-catalyzed azide-alkyne [3+2] cycloaddition, using THPTA as an activating agent.

Functionalizing the hydrogels with Kcoil, by improving the initial antibody capture (Figure 8A), allowed for the prolonged release of Ecoil-tagged antibodies during the late phase (24–96 h, Figure 8C, 100× and 1000×) compared to non-functionalized dextran gels.

This observation, consistent with results previously reported by Oliverio et al.,[15] indicates that tuning the Kcoil amount in gels allows fine control of capture and release behaviors for a given antibody. In this setup, the number and position of the E5 tags did not significantly affect the partition coefficients, meaning that all three antibodies behave similarly at equilibrium.

The cumulative release profiles (Figure 8B) showed that all three antibodies were quickly released from non-functionalized macroporous dextran hydrogels (black curves). Interestingly, at low (10×, red curves) and intermediate (100×, green curves) K5 densities, the three antibodies exhibit similar release profiles, with no statistically significant difference in terms of area under the curves (p > 0.05 in pairwise comparisons). However, at high K5 density (1000×, blue curves), HC5-LC5 displayed enhanced retention within the gel compared to the other E5coil-tagged TZM. The difference between the area under the curves for HC5-LC and HC-LC5 was not statistically significant (p > 0.05).

Altogether, we demonstrated that the number and position of the E5 tags did not significantly affect the capture of the modified TZM by macroporous dextran hydrogels. Furthermore, the number and position of the E5 tags did not affect the cumulative release, except at high Kcoil densities, where HC5-LC5 exhibited better retention.

Influence of the length of the Ecoil sequence on the capture and release of TZM by macroporous dextran hydrogels

We then explored another parameter to finely tune the levels of capture and release of Ecoil-tagged TZM from macroporous hydrogel: the length of the Ecoil sequence. We compared three antibodies: HC3-LC3, HC4-LC4 and HC5-LC5, that is, tetravalent Ecoil-tagged TZMs where the tags contained 3, 4 or 5 heptads (EVSALEK), respectively. We previously demonstrated by SPR biosensing (Figures 4 and 5, Table 3) that E3-, E4- and E5-tagged TZMs dissociated differently from grafted K5coil.

When measuring the capture of Ecoil-tagged TZMs by K5-functionalized gels (100×), we observed that decreasing the number of heptads decreases the partition coefficient (Figure 9A). In the case of HC3-LC3, no significant difference was observed between Dex and 100× conditions, which is consistent with the very low affinity observed in SPR between K5 and HC3-LC3. At the same time, we observed similar partition coefficient values for all three antibodies in non-functionalized dextran gels. This control confirms that the differences observed for the 100× conditions are indeed due to changes in the E/K interactions.

The same trends were observed for the release behaviors: while the cumulative release of HC5-LC5 reached about 55% of the initially loaded amount after 96 h, it reached about 80% for HC4-LC4 (Figure 9B). Moreover, pairwise comparisons of the area under the curves showed no difference between the release profiles from Dex and 100× gels for HC3-LC3. While 100× gels allowed for a prolonged release of HC5-LC5 and HC4-LC4 in the late phase (24 h – 96 h, Figure 9C), no difference was observed between Dex and 100× for HC3-LC3.
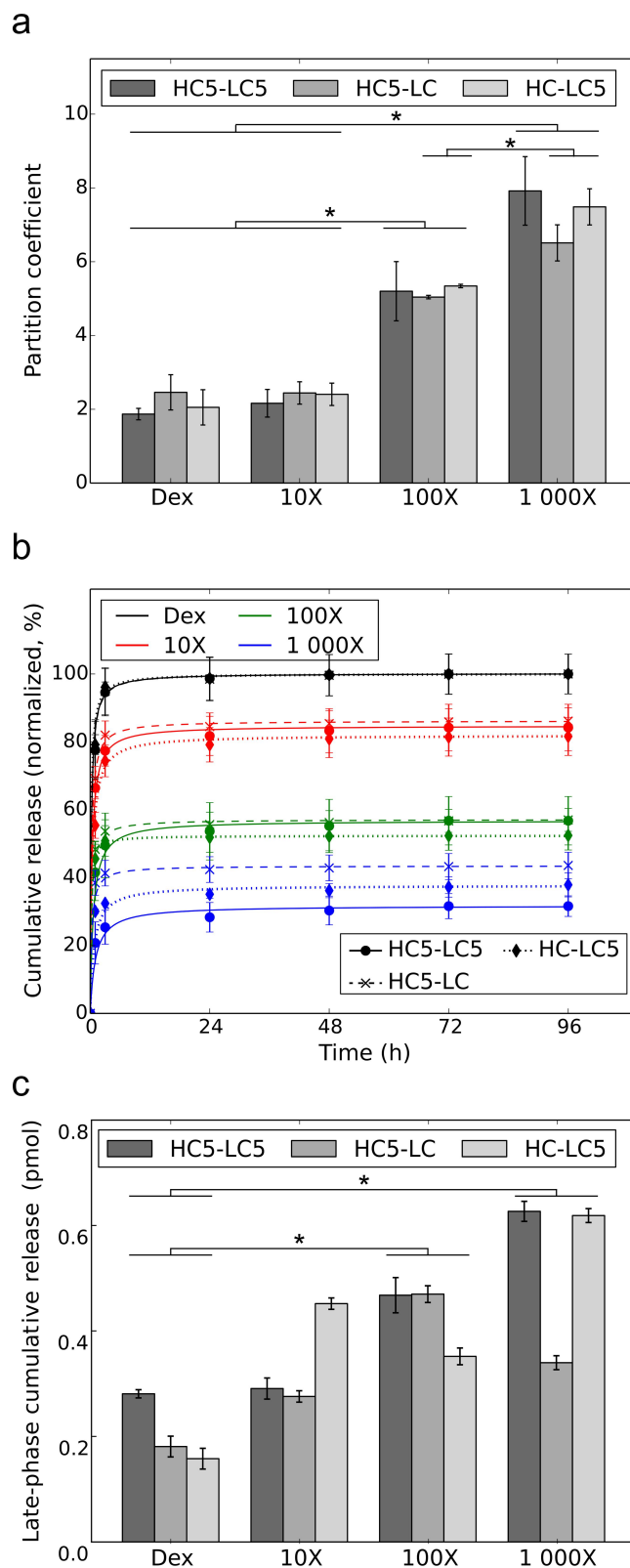
Figure 8. Influence of the number and position of the E5 tags on the capture and release of E5-tagged TZM by macroporous dextran hydrogels. (A) Partition coefficients characterizing HC5-LC5, HC5-LC and HC-LC5 distribution at equilibrium between the gels and the surrounding medium, for a grafted amount of K5 in the gels of 0 nmol (Dex), 0.5 nmol (10X), 5 nmol (100X) or 50 nmol (1000X). (B) Cumulative release of HC5-LC5 (round-shaped markers & full lines), HC5-LC (x-shaped markers & dashed lines) and HC-LC5 (diamond-shaped markers & dotted lines) by dextran hydrogels. Cumulative release is expressed as a percentage of the amount initially loaded in the gels, and data is normalized to 100%. Curves are hyperbolic fits displayed as guides for the eye. (C) Non-normalized, cumulative release during the 24 h − 96 h phase ("late-phase release"). Data is mean ± standard deviation, 6 measurements from $n=2$ independent experiments. * ($p < 0.05$) indicates statistically significant differences in pairwise comparisons (bilateral t-test). Some statistical annotations are omitted for the sake of figure readability.
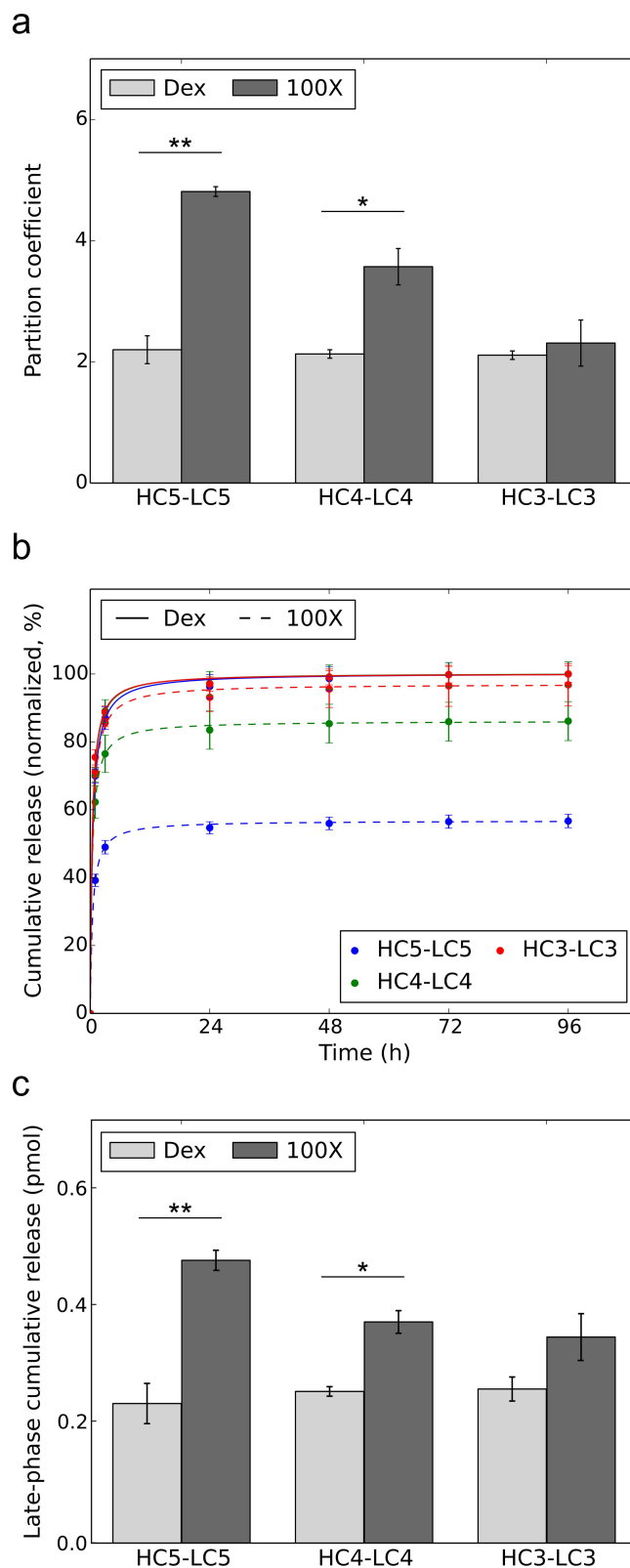
Figure 9. Influence of the length of the Ecoil tags on the capture and release of Ecoil-tagged TZM by macroporous dextran hydrogels. (A) Partition coefficients characterizing HC5-LC5, HC4-LC4 and HC3-LC3 distribution at equilibrium between the gels and the surrounding medium, for a grafted amount of K5 in the gels of 0 nmol (Dex) or 5 nmol (100X). (B) Cumulative release of HC5-LC5 (blue), HC4-LC4 (green) and HC3-LC3 (red) by dextran hydrogels. Cumulative release is expressed as a percentage of the amount initially loaded in the gels, and data is normalized to 100%. Curves are hyperbolic fits displayed as guides for the eye. (C) Non-normalized, cumulative release during the 24 h − 96 h phase ("late-phase release"). Data is mean ± standard deviation, 6 measurements from n=2 independent experiments. * ($p < 0.05$) and ** ($p < 0.01$) indicate statistically significant differences in pairwise comparisons (bilateral t-test). Some statistical annotations are omitted for the sake of figure readability.

Altogether, we have demonstrated here that the number of heptads of the Ecoil tags is a powerful tool to control the capture and release behaviors of Ecoil-tagged TZM from macroporous dextran hydrogels.

Discussion

Many studies have reported alternative routes of administration for mAbs, aiming to increase therapeutic efficacy, minimize drug exposure and improve patient compliance. The use of hydrogels for a controlled and sustained delivery is one of the strategies often explored.[9,11,12] In that endeavor, the E/K heterodimeric coiled-coil interaction exhibits interesting properties, making it a good candidate for the design of an affinity-based antibody delivery strategy.[15,23,34] The major goal of this work was thus to manufacture an Ecoil-tagged antibody (Ecoil-tagged TZM) and demonstrate its potential for controlled delivery applications.

Production of the coil-tagged proteins in mammalian expression systems has been reported.[35,36] Notably, Trang et al. reported *N*-terminal coiled-coil-tagged antibodies,[37] as a general approach for masking the complementary-determining regions of the selected mAbs. This approach allowed them to regulate the binding of the mAb to its antigen and improve the tumor targeting with an enhanced circulation half-life. They demonstrated that the presence of an adequate coiled-coil mask efficiently decreased the binding capacity of the selected mAbs to the cell surface antigens (750-fold decrease). After removal of the mask with proteases, the antibody-binding capacity was restored to that of the unmasked antibody. Although the coiled-coil tag was used for a different purpose than in this study, their work has shown that the addition of the coil motif to the backbone of the antibody does not hamper antibody folding.

In this study, where our aim was to preserve the binding capacity of the antibodies, we chose to position the Ecoil tags at the *C*-termini of the light and/or heavy chains. According to our experimental data (Table 1, Figure 2), the presence of the Ecoil tags did not hamper the antibody productions or drastically lowered the titers. The lowest production titers were 163 and 170 mg/L and were obtained for HC4-LC4 and HC5-LC5, respectively, while wild-type TZM had a titer of 217 mg/L. Production of recombinant proteins with genetically encoded affinity tags is sometimes challenging and certain aspects like length, degree of hydrophobicity and total net charge (positive or negative) should always be considered.[38–40] The lower production titers of HC4-LC4 and HC5-LC5 could be explained by the fact that the tags slightly increase the hydrophobicity and change the surface net charge of the molecules since the Ecoil tags contain hydrophobic and charged amino acids. These alterations can negatively affect the folding and/or secretion efficiency, resulting in a lower production titer. We hypothesize that this negative effect was not observed for the antibodies with 3 heptad repeat tags (HC3-LC3, HC3-L, H-LC3) due to the short length of the tag resulting in a smaller charge variation. Low production titers can also be caused by protein aggregates. The addition of the tag may compromise the final protein conformation and cause the formation of aggregates,[38] resulting in lower titers compared to the untagged proteins.

Furthermore, the driving force in the E/K coil system for homo- or heterodimerization mainly depends on the amino acids at the *e* and *g* positions, which are oppositely charged to form parallel heterodimers.[25] Despite this, some level of transient homodimerization of Kcoil and homotrimerization of Ecoil have been reported in several studies, especially when the coil is part of a fusion protein.[35,41,42] However, this homomerization is reversible upon addition of the complementary E or K coil, respectively. We believe that the addition of the E5 tags both in heavy and light chains may be responsible for increased protein aggregates and decrease in the production yield. Results from SEC-UPLC and SDS-PAGE (Table 1, Figure 2A, lane 2) for HC5-LC5 support this hypothesis.

For HC4-LC4, we observed a low titer value and detected some protein aggregates by SDS-PAGE (Figure S1). However, the level of aggregates analyzed by SEC-UPLC for this product was similar to other TZM variants and indicated high purity (97.9%, Table 1). These results may be due to experimental variability since we only performed the production once, and we did not investigate its repeatability. Additional production would be required to document the accurate effect of E5 and E4 tags on mAb production. Our initial results are, however, very promising for the manufacturability of Ecoil-tagged antibodies.

To study the effect of the Ecoil tags on the TZM ability to bind to its target, HER2, we performed two different assays. First, we used a cell-based assay (Figure 3, Table 2) to measure the affinity of free, in-solution Ecoil-tagged TZM for HER2. Then, after showing that E5- and E4-tagged TZM can be recruited by a Kcoil-functionalized SPR surface (Figures 4, 5), we demonstrated that captured Ecoil-TZM remained able to bind to HER2 (Figure 6).

For the cell-binding assay, the results of three independent repeats show that the addition of the Ecoil tag does not significantly ($p > 0.05$) alter the binding affinity of the tagged TZMs to their target antigen on the cell surface (Table 2), regardless of the number and position of the tags. This observation *a posteriori* legitimates our design with *C*-terminal tags on light, heavy or both chains.

These results are supported by the SPR assay (Figure 6), in which all E5-tagged antibodies can strongly and stably bind to HER2 when captured by a Kcoil-functionalized surface. Interestingly, we noticed that the same amount of HC5-LC and HC-LC5 on the chip (95 RU) led to the capture of lower levels of HER2 for HC-LC5, i.e., when the Ecoil tags are grafted by the light chains only. In this experimental setup, the K5 surface coverage is very high, 1300 RU, which represents an average distance of 2 nm between two K5 moieties, allowing for two Ecoils on the same antibody to simultaneously bind to the Kcoil layer. We hypothesize that, in this particular configuration, the simultaneous capture of TZM by the two tags present on the light chains (Figure 1) can lead to the partial burial of the antigen-binding fragments within the Kcoil layer, thus partially preventing their availability to bind to HER2. When taken together, cell-based and SPR assays show that the ability of Ecoil-tagged TZMs to bind to its biological target HER2 is preserved. However, the choice of the number and position of the tags might be context dependent for optimal results.

We then studied how the number, position, and length of the Ecoil tags affected the capture and release of TZM by macroporous, Kcoil-functionalized dextran hydrogels. Interestingly, except at very high Kcoil densities (1000 ×), no significant difference was observed when comparing the capture and subsequent release of divalent HC5-LC and HC-LC5 on the one hand and tetravalent HC5-LC5, on the other hand, (Figure 8). This observation strongly contrasts with previous results from our group,[15] in which we recently reported a major influence of the number of Ecoils upon protein capture and release with Kcoil functionalized macroporous hydrogels, i.e., higher partition coefficients and slower release for Ecoil-tagged VEGF – two E5-tags – than for Ecoil-tagged EGF – one E5-tag. Murschel et al. measured the apparent thermodynamic dissociation constants for both K5/E5-EGF ($K_{D,app} = 0.2nM$) and K5/E5-VEGF ($K_{D,app} = 0.1pM$), evidencing a 1000-fold difference in $K_{D,app}$ between the two Ecoil-tagged growth factors, that is, a strong effect of the Ecoil valency.[43] The low $K_{D,app}$ of E5-VEGF was mainly due to the very low kinetic dissociation rate constant, with little to no dissociation observed in the SPR within 20 min of buffer injection[36] However, for E5-tagged TZM, we have shown that increasing the number of the tags from 2 to 4 only leads to a 2-fold decrease in the kinetic rate dissociation constant $k_{off,app}$ (Figure 4, Table 3): in that case, the effect of the Ecoil valency on the interaction is moderate. Altogether, our data suggest that the influence of the valency of Ecoil-tagged antibodies upon their capture and release behaviors in microporous gels can be anticipated from SPR experiments.

The SPR characterization of the Ecoil-tagged TZMs can also shed light upon behaviors illustrated in Figure 9, where we studied the influence of the Ecoil length on the capture and release behaviors. For HC3-LC3, both non-functionalized (Dex) and Kcoil-functionalized (100×) gels exhibited similar partition coefficient and release profiles, indicating that a 3-heptad-long Ecoil tag is not enough for an affinity-based controlled release in this experimental configuration. This observation is consistent with the SPR data (Figure S2) that shows that E3-tagged antibodies fail to bind to an SPR sensor chip functionalized with low amounts of K5 peptide (15 RUs). Altogether, Kcoil-functionalized macroporous hydrogels were shown to be an interesting tool for the controlled capture and release of mAbs. The release profiles (Figures 8B, 9B) exhibited two phases: 1) a phase of rapid release during the initial 24 h (three buffer changes); and 2) a steady, prolonged phase associated with a very low release rate (Figures 8C, 9C).

In agreement with our previous observations and subsequent hypothesis,[15] we believe that the first phase most likely corresponds to the release of antibodies that are physically present in the macropores, without being effectively bound to the macropore surface via a coiled-coil interaction. Once this initial phase is over, the strong, stable E/K interaction allows for the very slow dissociation of Ecoil-tagged TZM (Figures 8B-B, 9B-C). It is worth noting here that in our SPR experiments, complete Ecoil-tagged antibody dissociation from the Kcoil-decorated sensor surface had only been achieved with the injection of a strong chaotropic

solution (6 M guanidine hydrochloride) (Figures 4A-C, 5A-C). Such a strong interaction is required for efficiently slowing the release from macroporous dextran hydrogels. Indeed, once detached from the Kcoil layer and released in the macropores, the antibodies are not retained by the dextran mesh and can diffuse freely out of the gel.

Altogether, all experiments presented here show that since all Ecoil-tagged TZM retain their ability to bind their biological partner HER2, the choice of the number, length, and position of the Ecoil tags only depends on the desired application and the manufacturability of the Ecoil-tagged antibody. For example, in the case of the capture and release experiments, the presence of four tags instead of two does not improve the efficiency of the macroporous dextran hydrogels. Since HC5-LC5 exhibited higher amounts of aggregates and had therefore a lower purity than its E5-tagged counterparts (Table 1), HC5-LC and HC-LC5 should be favored in that situation.

In this work, we reported the manufacture of an Ecoil-tagged mAb (trastuzumab) to be feasible, and the chimeric antibody to retain its ability to bind to its cell surface antigen. More precisely, adding Ecoil tags at the C-termini of the antibody chains, regardless of the number and position of the tags (i.e., on the heavy and/or light chains), had limited impact upon antibody interaction with its antigen. As a proof-of-concept, we further used Ecoil-tagged TZM to develop an affinity-based release system from macroporous dextran hydrogels, taking advantage of the E/K coiled-coil system. For that application, we demonstrated that at least four heptads are required for the Ecoil-tagged antibodies to efficiently interact with the gel-immobilized Kcoil.

Altogether, the presented approach is versatile and could be applied to other mAbs for many different therapeutic applications. Future experimental work would focus on the therapeutic potential of the sustained release of Ecoil-tagged antibodies from macroporous hydrogels *in vivo*. Alternatively, the Ecoil tag system reported here can function as a specific and universal attachment site for producing labeled antibodies and therapeutic compound-antibody conjugates, expanding the range of potential applications in research, diagnostics, and therapeutics.

Materials and methods

Expression vectors

The pTT5® vectors[44] containing wild-type trastuzumab (TZM) heavy (HC) and light chain (LC) DNA sequences were double digested by *Bsr*GI-*Bgl*II and *Eco*RI-*Dra*III restriction enzymes, respectively, to insert the Ecoil DNA fragment. The resulting plasmids, coding for the TZM HC or LC bearing a C-terminal Ecoil tag will be referred to as pTT5-HCx and pTT5-LCx, respectively, where x (3, 4 or 5) stands for the number of heptads. Proper insertion of the Ecoil sequences was verified by sequencing (Applied Biosystems Abi 3500 ×l DNA Sequencer – LabX). pTTo-GFP (green fluorescence reporter gene) and pTT22-hAktDD (constitutively active Akt mutant) were co-transfected as previously described.[45,46]

Cell culture and transient gene expression

Ecoil-tagged mAbs were produced by transient gene expression (TGE) in CHO-3E7 cells according to a modified version of a previously described protocol.[29,47] CHO-3E7 cells, maintained in FreeStyle F17 medium (Invitrogen, cat# A13835–01) supplemented with 4 mM glutamine (Sigma-Aldrich, cat# G8540) and 0.1% Kolliphor P188 (Sigma-Aldrich, cat# K4894), were seeded 24 h before transfection to reach a density of $2.0–2.2 \times 10^6$ cells/ml at the time of transfection. The transfected DNA was a mix of heavy chain (pTT5-HC or pTT5-HCx) and light chain (pTT5-LC or pTT5-LCx) plasmids at a ratio of 1:2 (80% [w:w]), pTTo-GFP (5%[w:w]), and pTT22-hAktDD (15%[w:w]).

Plasmid DNA and polyethyleneimine (PEI) (PEI max, PolySciences, cat# 24765) were diluted separately in F17 medium to reach a final concentration of 1.0 µg/ml and 4.0 µg/ml, respectively. Diluted PEI was added to diluted DNA and incubated for 5–7 min at room temperature. The mixture was then added to the cells, and the flasks were incubated under constant agitation (120 rpm) at 37°C, 5% CO_2 (standard humidity conditions). Twenty-four hours post-transfection (hpt), cultures were supplemented with Tryptone N1 (1% [w/v], Organotechnie), valproic acid (0.5 mM, Sigma Aldrich, cat# P4543) and 14 mM glucose (Sigma Aldrich, cat# G7021) and further incubated at 32°C under the same agitation, CO_2 and humidity conditions. The transfection efficiency was assessed 48 hpt by determining the percentage of GFP positive cells compared to non-transfected CHO-3E7 cells by dual-fluorescence imaging with a Cellometer K2 cell counter (Nexcelom Bioscience). Only viable single cells were considered.

Subsequently, cell count and cell viability were monitored every 2–3 days using a CEDEX (Innovatis) automated cell counter. Glucose and lactate concentrations were also measured, using an YSI 2500 instrument (Xylem). Cells were supplemented when needed with glucose to maintain their concentration above 12 mM. Ten days post transfection, the cultures were stopped (viability >70%) and centrifuged (40 min, 4000 g). The clarified supernatants were collected and filter-sterilized using a 0.22 µm membrane vacuum filter (Express PLUS, Millipore).

Purification of Ecoil-tagged TZMs

Filtered supernatants were loaded on MabSelect SuRe (GE Healthcare, cat# 17–5438–02) columns equilibrated in PBS. The columns were washed with PBS, and proteins were eluted with 100 mM citrate buffer (pH 3.6). The fractions containing eluted chimeric mAbs were pooled and elution buffer was exchanged for PBS using CentriPure *P*-100 desalting columns (emp Biotech GmbH, Germany). Final mAb titers in culture supernatants were determined by protein-A HPLC using an 800 µl POROS 20 µm Protein A ID Cartridge (Applied Biosystems, cat# 2–1001–00) according to the manufacturer's recommendations. Purified proteins in PBS were quantified by absorbance at 280 nm using a Nanodrop spectrophotometer (Thermo Fisher Scientific) and the calculated extinction coefficient for each protein (ProtParam tool – Expasy). Purified mAbs were sterilized by passing through 0.2 mm filters, aliquoted, and stored at −80°C.

Characterization of Ecoil-tagged TZMs

SDS-PAGE

SDS-PAGE was performed in reducing and non-reducing conditions using NuPAGE 4–12% Bis-Tris gels (Invitrogen). Protein samples were diluted in reducing (resp. non-reducing) sample buffer (4× Laemmli, BioRad) and then denatured at 70°C for 10 min. The samples migrated in the gels for 55 min at 200 V, using 3-(N-morpholino) propanesulfonic acid (MOPS) as the running buffer. 10 µl BioRad precision plus standard was used as a molecular weight marker for each gel. The total protein content was revealed by Coomassie Blue R250 staining.

UPLC SEC-MALS

UPLC-SEC – MALS analyses were conducted on the final products using a 4.6×150 mm BEH200 SEC column with 1.7 µm particles (Waters, Milford, MA) connected to an Acquity H-Class Bio UPLC system (Waters) with a miniDAWN MALS detector and an Optilab T-rEX refractometer (Wyatt Technology, Santa Barbara, CA, USA). The column temperature was 30°C and the mobile phase was Dulbecco's PBS (HyClone SH30028.01) with 0.02% Tween 20. The flow rate was 0.4 mL/min. Weighted average molecular mass (M_{MALS}) was calculated in ASTRA 6.1 software (Wyatt) using a protein concentration determined from the refractive index signal, considering a dn/dc value of 0.185.

Cell binding assay on HER2 expressing cell line

SK-BR-3 cells were seeded in 96-well plates (7200 cells per well in 50 µl culture medium) and grown overnight. Triple-negative breast cancer cell line MDA-MB-231 was used as negative control. Plates were cooled to 4°C and 50 µl of the Ecoil tagged TZM dilutions (014–300 nM) in DPBS were added and incubated for 2 hours at 4°C followed by a wash (D-PBS with Ca^{2+}, Mg^{2+}, 4°C). Same dilutions of TZM and palivizumab were added as the positive and negative controls, respectively. Afterward, 25 µl of the secondary antibody solution containing anti-human (H+L) AF488-labeled IgG (1:200 v/v dilution; Jackson ImmunoResearch Labs, cat# 309-545-082), nuclear dye Hoechst 33,342 (1:2000 v/v dilution, Molecular Probes, cat# H3750) and CellMask Deep Red Plasma Membrane Stain (1:1000 v/v dilution, Thermo Fisher Scientific, cat# C10046) was added to each well and incubated for 1 h at 4°C. After a quick wash (D-PBS with Ca^{2+}, Mg^{2+}, 4°C), cell images were captured (ImageXpress Micro (IXM) Widefield High Content Imaging System; Molecular Devices), processed (MetaXpress software; Molecular Devices), and further analyzed using GraphPad Prism v8 software by a One site – specific binding model to determine the maximum specific binding B_{max} and the apparent thermodynamic dissociation constant K_D.

Surface plasmon resonance assays

SPR assays were performed on a Biacore T100 or T200 biosensor (Cytiva), using CM5 sensor chips (Cytiva). The running buffer was HBS-EP (0.01 M HEPES pH 7.4, 0.15 M sodium chloride, 3 mM ethylenediamine tetraacetic acid (EDTA) and 0.005% v/v P20 surfactant). All sensorgrams were acquired at 37°C, with an acquisition rate of 10 Hz. Samples were injected on a mock, non-functionalized surface, and on the working surface. Prior to the analysis, sensorgrams were double referenced by subtracting to the sample signal: 1) the signal measured on the mock surface and 2) the signal obtained when only buffer is injected. All analyses are performed using the BiaEvaluation 3.1 software (Cytiva).

The CM5 chips were functionalized as previously described.[36] Briefly, the carboxyl groups were activated using N-hydroxysuccinimide and 1-ethyl-3-(3-dimethyl aminopropyl) carbodiimide, allowing for the grafting of the thiol-reactive PDEA ligand (Cytiva) by amine coupling. The remaining carboxyl groups were then blocked with 1 M ethanolamine (pH 8.5).

Interaction of Ecoil-tagged TZM with Kcoil

Fifteen resonance units (RU) of cysteine-tagged Kcoil (KVSALKE)$_5$-GGC were then immobilized on the working surface only and the remaining reactive groups were blocked using L-cysteine, on both the working surface and the mock surface. Then, 2.5, 5, 10, 25 and 50 nM of HC5-LC5, HC5-LC, HC-LC5 or 25, 50, 100, 250 and 500 nM of HC4-LC4, LC4-LC, HC-LC4 in HBS-EP were injected on both surfaces at 50 μL/min for 240 s, followed by 3600 s of HBS-EP only. Surfaces were regenerated by injecting three 15 s pulses of 6 M guanidine hydrochloride. All injections were performed in duplicates.

Interaction of HER2 with Ecoil-tagged TZM

One thousand three hundred RU of cysteine-tagged Kcoil were immobilized on both mock and working surfaces. The remaining thiol-reactive groups were then blocked using L-cysteine. HC5-LC5, HC5-LC or HC-LC5 (75 RU, 95 RU or 95 RU, respectively) in HBS-EP were then injected on the working surface only. 3, 10 and 25 nM of HER2 (eBiosciences) in HBS-EP were injected on both surfaces at 40 μL/min for 100 s, followed by 600 s of HBS-EP only. Surfaces were regenerated by injecting three 15 s pulses of 6 M guanidine hydrochloride, and all injections were performed in duplicates.

Macroporous dextran gels synthesis

Macroporous dextran hydrogels were synthesized, as previously described,[15] by molding and crosslinking dextran on macroporous PLA scaffolds. Briefly, extruded rods of co-continuous polystyrene (PS)/PLA blends were annealed using a hot press, for 60 min at 190°C. The rods were then cut (quarters of cylinders, 4–6 mm height and 5–8 mm radius), and the PS

phase was selectively dissolved in cyclohexane. The obtained PLA scaffolds have a macropore size of 200 ± 100 μm.[15]

Dextran *T*-500 (Pharmacosmos, 200 mg/mL) and STMP (Sigma #T5508, 40 mg/mL) were dissolved in ultrapure water. The solution was then supplemented with sodium hydroxide to reach a final concentration of 1 M NaOH and was injected into the PLA scaffolds by nitrogen/vacuum cycles. The PLA scaffolds filled with dextran were then incubated for 15 min at 50°C to allow for dextran crosslinking. They were then immersed in chloroform until complete dissolution of the PLA, leading to macroporous dextran hydrogels. The gels were then immersed in PBS, pH 7.4 overnight. The hydrogels had a macropore size of 400 ± 200 μm at swelling equilibrium.[15]

Macroporous dextran gels functionalization

The Kcoil peptide (sequence: AhaGG-(KVSALKE)$_5$, where Aha stands for the non-natural amino acid azidohomoalanine) was conjugated to dextran using copper-catalyzed azide-alkyne cycloaddition,[48] as previously described.[15] Briefly, the gels were first incubated overnight at 37°C in a solution containing 200 nmol of glycidyl propargyl ether (GPE) in 200 mM NaOH. The gels were then extensively rinsed in PBS until reaching a pH of 7.4. This first step allows the functionalization of the dextran backbone with alkyne moieties. Then, the gels were immersed in a degassed PBS solution containing 0, 0.5, 1.5, 5, 15 or 50 nmol of Kcoil. Tris(3-hydroxypropyltriazolylmethyl)amine (THPTA) (Sigma #762342) and copper sulfate pentahydrate (Sigma #C8027) were premixed in ultrapure water and degassed, then added to the reaction mix to reach final concentrations of 2 mM and 0.4 mM, respectively. The solution was then supplemented twice with sodium ascorbate (Sigma #A4034) in PBS (degassed): first, to start the reaction (5 mM sodium ascorbate in the reaction mix), then a second time after 24 h (10 mM sodium ascorbate). The reaction was carried on for 48 h, at room temperature, protected from light. Upon completion of the reaction, the gels were rinsed extensively for 24 h: twice with PBS +10 mM EDTA to remove copper, then three times with PBS only.

Capture and release assays

Capture

Macroporous dextran gels were immersed in 1 mL ($V_{solution}$) of a solution containing 50 nM ($C_{solution,init}$) Ecoil-tagged TZM, at 37°C on a shaking platform. The buffer was PBS supplemented with 0.05% v/v Tween-20 (PBS-T). After 72 h, the solution was collected and replaced by 1 mL fresh PBS-T ($t = 0$ h).

Release

At $t = 1, 3, 24, 48$ and 96 h, the solution surrounding the gels was collected and replaced by fresh PBS-T. Between medium changes, the gels were incubated at 37°C, on a shaking platform.

Analysis

The ability of the gels to capture Ecoil-tagged TZM was quantified by the partition coefficient P (5). P characterizes the

distribution of the Ecoil-tagged TZM between the pores of the gel and the surrounding medium after the initial 72 h incubation.

$$P = \frac{C_{gel}}{C_{solution}} = \frac{(C_{solution,init} - C_{solution}) \cdot V_{solution}}{C_{solution} \cdot V_{pores}} \quad (5)$$

V_{pores} represents the volume of the macropores and is obtained by weighing the gels twice: once with pores full, and once after emptying the pores by capillarity with a Kimwipe. The difference between the two values is converted to a volume assuming a volumetric mass density of 1 g/mL for PBS-T.

$C_{solution}$ is the concentration of the solution after the initial 72 h incubation and is measured by an anti-hIgG Enzyme-Linked Immunosorbent Assay (ELISA) (capture antibody: Jackson ImmunoResearch #109-005-008, detection antibody: #109-035-003).

Similarly, the release media collected after 1, 3, 24, 48, 72 and 96 h were analyzed by ELISA. The obtained concentrations were used to draw the Ecoil-tagged TZM release profiles.

Abbreviations

CHO	Chinese hamster ovary
EGF	Epidermal Growth Factor
ELISA	enzyme-linked immunosorbent assay
GPE	glycidyl propargyl ether
HC	heavy chain
HER2	Human Epidermal growth factor Receptor 2
HPLC	high-performance liquid chromatography
hpt	hours post transfection
LC	light chain
mAb	monoclonal antibody
MALS	multi-angle light scattering
PEI	polyethyleneimine
PLA	polylactic acid
PS	polystyrene
PVZM	palivizumab
RU	resonance units
SDS-PAGE	sodium dodecyl sulfate – polyacrylamide gel electrophoresis
SEC	size-exclusion chromatography
SPR	surface plasmon resonance
STMP	trisodium trimetaphosphate
THPTA	tris-hydroxypropyltriazolylmethylamine
TZM	trastuzumab
UPLC	ultra-performance liquid chromatography
VEGF	Vascular Endothelial Growth Factor

Acknowledgments

Disclosure statement

Funding

ORCID

Yves Durocher 🔾 http://orcid.org/0000-0002-2268-4111

References

1. Castelli MS, McGonigle P, Hornby PJ. The pharmacology and therapeutic applications of monoclonal antibodies. Pharmacol Res Perspect. 2019;7(6):e00535. doi:10.1002/prp2.535.
2. Yamada T. Therapeutic monoclonal antibodies. Keio J Med. 2011;60(2):37–46. doi:10.2302/kjm.60.37.
3. Jin S, Sun Y, Liang X, Gu X, Ning J, Xu Y, Chen S, Pan L. Emerging new therapeutic antibody derivatives for cancer treatment. Sig Transduct Target Ther. 2022;7:39. doi:10.1038/s41392-021-00868-x.
4. Schellekens H. Bioequivalence and the immunogenicity of biopharmaceuticals. Nat Rev Drug Discov. 2002;1:457–62. doi:10.1038/nrd818.
5. Cui Y, Cui P, Chen B, Li S, Guan H. Monoclonal antibodies: formulations of marketed products and recent advances in novel delivery system. Drug Dev Ind Pharm. 2017;43(4):519–30. doi:10.1080/03639045.2017.1278768.
6. Wang W, Wang EQ, Balthasar JP. Monoclonal antibody pharmacokinetics and pharmacodynamics. Clin Pharmacol Ther. 2008;84:548–58. doi:10.1038/clpt.2008.170.
7. Huynh V, Wylie RG. Competitive affinity release for long-term delivery of antibodies from hydrogels. Angew Chem Int Ed Engl. 2018;57(13):3406–10. doi:10.1002/anie.201713428.
8. Chen M, Ouyang H, Zhou S, Li J, Ye Y. PLGA-nanoparticle mediated delivery of anti-OX40 monoclonal antibody enhances anti-tumor cytotoxic T cell responses. Cell Immunol. 2014;287(2):91–99. doi:10.1016/j.cellimm.2014.01.003.
9. Fletcher NA, Babcock LR, Murray EA, Krebs MD. Controlled delivery of antibodies from injectable hydrogels. Mater Sci Eng

C Mater Biol Appl. 2016;59:801–06. doi:10.1016/j.msec.2015.10.096.

10. Booth BA, Vidal Denham L, Bouhanik S, Jacob JT, Hill JM. Sustained-release ophthalmic drug delivery systems for treatment of macular disorders: present and future applications. Drugs Aging. 2007;24(7):581–602. doi:10.2165/00002512-200724070-00006.

11. Huynh V, Jesmer AH, Shoaib MM, D'Angelo AD, Rullo AF, Wylie RG. improved efficacy of antibody cancer immunotherapeutics through local and sustained delivery. Chembiochem. 2019;20:747–53. doi:10.1002/cbic.201800579.

12. Cirillo G, Spizzirri UG, Curcio M, Nicoletta FP, Iemma F. Injectable hydrogels for cancer therapy over the last decade. Pharmaceutics. 2019;9:11. doi:10.3390/pharmaceutics11090486.

13. De France KJ, Xu F, Hoare T. Structured macroporous hydrogels: progress, challenges, and opportunities. Adv Healthcare Mater. 2018;7(1):1700927. doi:10.1002/adhm.201700927.

14. Dinu MV, ES D. Macroporous hydrogels: preparation, properties, and applications. In: Thakur V Thakur M, editors. Hydrogels: Recent advances. Singapore:Springer Singapore; 2018. pp. 51–85. 10.1007/978-981-10-6077-9_3

15. Oliverio R, Patenaude V, Liberelle B, Virgilio N, Banquy X, De Crescenzo G. Macroporous dextran hydrogels for controlled growth factor capture and delivery using coiled-coil interactions. Acta Biomater. 2022. doi:10.1016/j.actbio.2022.09.020.

16. Carasso LS, Benhar I, Dvir T. Universal biofactor-releasing scaffold enabling in vivo reloading. Nano Lett. 2019;19(3):1838–43. doi:10.1021/acs.nanolett.8b04927.

17. Utterstrom J, Naeimipour S, Selegard R, Aili D. Coiled coil-based therapeutics and drug delivery systems. Adv Drug Deliv Rev. 2021;170:26–43 doi:10.1016/j.addr.2020.12.012.

18. Abune L, Wang Y. Affinity hydrogels for protein delivery. Trends Pharmacol Sci. 2021;42:300–12. doi:10.1016/j.tips.2021.01.005.

19. Vulic K, Shoichet MS. Tunable growth factor delivery from injectable hydrogels for tissue engineering. J Am Chem Soc. 2012;134(2):882–85. doi:10.1021/ja210638x.

20. Abune L, Zhao N, Lai J, Peterson B, Szczesny S, Wang Y. Macroporous hydrogels for stable sequestration and sustained release of vascular endothelial growth factor and basic fibroblast growth factor using nucleic acid aptamers. ACS Biomaterials Science & Engineering. 2019;5(5):2382–90. doi:10.1021/acsbiomaterials.9b00423.

21. Huynh V, Wylie RG. Competitive affinity release for long-term delivery of antibodies from hydrogels. Angewandte Chemie International Edition. 2018;57(13):3406–10. doi:10.1002/anie.201713428.

22. Huynh V, Wylie RG. Displacement affinity release of antibodies from injectable hydrogels. ACS Appl Mater Interfaces. 2019;11(34):30648–60. doi:10.1021/acsami.9b12572.

23. Mason JM, Arndt KM. Coiled coil domains: stability, specificity, and biological implications. Chembiochem. 2004;5:170–76. doi:10.1002/cbic.200300781.

24. Litowski JR, Hodges RS. Designing heterodimeric two-stranded α-helical coiled-coils. J Biol Chem. 2002;277(40):37272–79. doi:10.1074/jbc.M204257200.

25. Apostolovic B, Danial M, Klok HA. Coiled coils: attractive protein folding motifs for the fabrication of self-assembled, responsive and bioactive materials. Chem Soc Rev. 2010;39(9):3541–75. doi:10.1039/b914339b.

26. Truebestein L, TA L. Coiled-coils: the long and short of it. Bioessays. 2016;38(9):903–16. doi:10.1002/bies.201600062.

27. Woolfson DN. Coiled-coil design: updated and upgraded. Subcell Biochem. 2017;82:35–61 doi:10.1007/978-3-319-49674-0_2.

28. Surkont J, Pereira-Leal JB. Evolutionary patterns in coiled-coils. Genome Biol Evol. 2015;7(2):545–56. doi:10.1093/gbe/evv007.

29. Raymond C, Robotham A, Spearman M, Butler M, Kelly J, Durocher Y. Production of α2,6-sialylated IgG1 in CHO cells. MAbs. 2015;7(3):571–83. doi:10.1080/19420862.2015.1029215.

30. Liu H, Gaza-Bulseco G, Chumsae C, Newby-Kew A. Characterization of lower molecular weight artifact bands of recombinant monoclonal IgG1 antibodies on non-reducing SDS-PAGE. Biotechnol Lett. 2007;29(11):1611–22. doi:10.1007/s10529-007-9449-8.

31. Zhang Y, Wang Y, Li Y. Major cause of antibody artifact bands on non-reducing SDS-PAGE and methods for minimizing artifacts. Protein Expr Purif. 2019;164:105459. doi:10.1016/j.pep.2019.105459.

32. Zhu ZC, Chen Y, Ackerman MS, Wang B, Wu W, Li B, Obenauer-Kutner L, Zhao R, Tao L, Ihnat PM. Investigation of monoclonal antibody fragmentation artifacts in non-reducing SDS-PAGE. J Pharmaceut Biomed. 2013;83:89–95. doi:10.1016/j.jpba.2013.04.030.

33. Stenberg E, Persson B, Roos H, Urbaniczky C. Quantitative determination of surface concentration of protein with surface plasmon resonance using radiolabeled proteins. J Colloid Interface Sci. 1991;143:513–26. doi:10.1016/0021-9797(91)90284-F.

34. De Crescenzo G, Litowski JR, Hodges RS, O'Connor-McCourt MD. Real-time monitoring of the interactions of two-stranded de novo designed coiled-coils: effect of chain length on the kinetic and thermodynamic constants of binding. Biochemistry. 2003;42:1754–63. doi:10.1021/bi0268450.

35. Fernandez-Rodriguez J, Marlovits TC. Induced heterodimerization and purification of two target proteins by a synthetic coiled-coil tag. Protein Sci. 2012;21(4):511–19. doi:10.1002/pro.2035.

36. Murschel F, Liberelle B, St-Laurent G, Jolicoeur M, Durocher Y, De Crescenzo G. Coiled-coil-mediated grafting of bioactive vascular endothelial growth factor. Acta Biomater. 2013;9(6):6806–13. doi:10.1016/j.actbio.2013.02.032.

37. Trang VH, Zhang X, Yumul RC, Zeng W, Stone IJ, Wo SW, Dominguez MM, Cochran JH, Simmons JK, Ryan MC, et al. A coiled-coil masking domain for selective activation of therapeutic antibodies. Nat Biotechnol. 2019;37(7):761–65. doi:10.1038/s41587-019-0135-x.

38. Pina AS, Lowe CR, Roque AC. Challenges and opportunities in the purification of recombinant tagged proteins. Biotechnol Adv. 2014;32(2):366–81. doi:10.1016/j.biotechadv.2013.12.001.

39. Lienqueo ME, Salazar O, Calado CR, Fonseca LP, Cabral JM. Influence of tryptophan tags on the purification of cutinase, secreted by a recombinant Saccharomyces cerevisiae, using cationic expanded bed adsorption and hydrophobic interaction chromatography. Biotechnol Lett. 2008;30:1353–58. doi:10.1007/s10529-008-9696-3.

40. Bernier SC, Cantin L, Salesse C. Systematic analysis of the expression, solubility and purification of a passenger protein in fusion with different tags. Protein Expr Purif. 2018;152:92–106. doi:10.1016/j.pep.2018.07.007.

41. Gerling-Driessen UI, Mujkic-Ninnemann N, Ponader D, Schöne D, Hartmann L, Koksch B, Gerling-Driessen UI, Schöne D, Koksch B, Ponader D, et al. Exploiting oligo(amido amine) backbones for the multivalent presentation of coiled-coil peptides. Biomacromolecules. 2015;16(8):2394–402. doi:10.1021/acs.biomac.5b00634.

42. Apostolovic B, Klok HA. Ph-sensitivity of the E3/K3 heterodimeric coiled coil. Biomacromolecules. 2008;9:3173–80. doi:10.1021/bm800746e.

43. Murschel F, Fortier C, Jolicoeur M, Hodges RS, De Crescenzo G. Two complementary approaches for the controlled release of biomolecules immobilized via coiled-coil interactions: peptide core mutations and multivalent presentation. Biomacromolecules. 2017;18:965–75. doi:10.1021/acs.biomac.6b01830.

44. Durocher Y, Perret S, Kamen A. High-level and high-throughput recombinant protein production by transient transfection of suspension-growing human 293-EBNA1 cells. Nucleic Acids Res. 2002;30:E9. doi:10.1093/nar/30.2.e9.

45. Dorion-Thibaudeau J, Raymond C, Lattová E, Perreault H, Durocher Y, De Crescenzo G. Towards the development of a surface plasmon resonance assay to evaluate the glycosylation pattern of monoclonal antibodies using the extracellular domains

of CD16a and CD64. J Immunol Methods. 2014;408:24–34. doi:10.1016/j.jim.2014.04.010.

46. Dorion-Thibaudeau J, St-Laurent G, Raymond C, De Crescenzo G, Durocher Y. Biotinylation of the Fcγ receptor ectodomains by mammalian cell co-transfection: application to the development of a surface plasmon resonance-based assay. Journal Of Molecular Recognition. 2016;29(2):60–69. doi:10.1002/jmr.2495.

47. Delafosse L, Xu P, Durocher Y. Comparative study of polyethyle-nimines for transient gene expression in mammalian HEK293 and CHO cells. J Biotechnol. 2016;227:103–11. doi:10.1016/j.jbiotec.2016.04.028.

48. Presolski SI, Hong VP, Finn M. Copper-catalyzed azide–alkyne click chemistry for bioconjugation. Curr Protoc Chem Biol. 2011;3:153–62. doi:10.1002/9780470559277.ch110148.